Supporting Information

Ternary alloyed $AgCl_xBr_{1-x}$ nanocrystals: facile modulation of electronic structure toward advanced photocatalytic performance

Bin Cai,[a,c] Jing Wang,[b,c] Dongxue Han,*[a] Shiyu Gan,[a,c] Qixian Zhang,[a] Zhijian Wu,[b] and Li Niu[a]

[a] *State Key Laboratory of Electroanalytical Chemistry, c/o Engineering Laboratory for Modern Analytical Techniques, Changchun Institute of Applied Chemistry, Chinese Academy of Sciences, Changchun 130022, Jilin, China. E-mail: lniu@ciac.jl.cn*

[b] *State Key Laboratory of Rare Earth Resource Utilization, Changchun Institute of Applied Chemistry, Chinese Academy of Sciences, Changchun 130022, Jilin, China.*

[c] *Graduate University of the Chinese Academy of Sciences, Beijing 100039, China.*

I. Experimental Details

A. Synthesis of $AgCl_xBr_{1-x}$ NCs

The chloroform solution of CTAC/CTAB with proportional concentration is presented in Table S1.

Table S1 Chloroform solutions with different CTAC/CTAB concentration ratios (mol L^{-1})

Samples	AgCl	$AgCl_{0.75}Br_{0.25}$	$AgCl_{0.5}Br_{0.5}$	$AgCl_{0.25}Br_{0.75}$	AgBr
CTAC	0.04	0.03	0.02	0.01	0
CTAB	0	0.01	0.02	0.03	0.04

B. The photoreduction of CO_2 into methanol and ethanol

The home-made reactor for photoreduction of CO_2 into methanol and ethanol is illustrated in Figure S1.

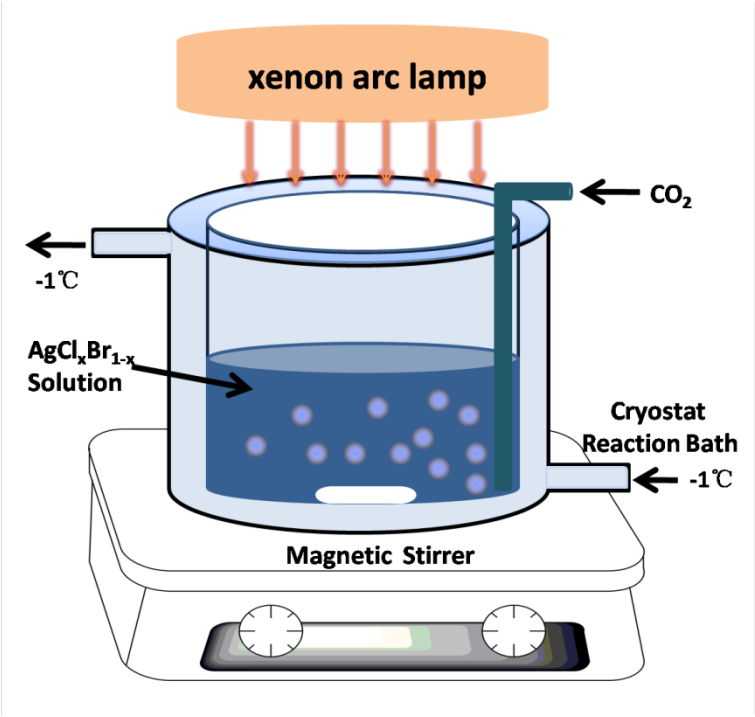

Figure S1 Schematic diagram of the home-made photocatalytic reduction system.

C. The calculation of apparent quantum efficiency

The CO_2 photoreduction undergoes two kinds of typical reaction processes as follows: $CO_2 + 6H^+ + 6e^- \rightarrow CH_3OH + H_2O$ and $2CO_2 + 12H^+ + 12e^- \rightarrow C_2H_5OH + 3H_2O$. Thus the apparent quantum efficiency could be calculated as the following equation (1),

$$QE\ (\%) = \frac{N_{electrons}}{N_{photons}} \times 100\% = \frac{N_{methaol} \times 6 + N_{ethanol} \times 16}{N_{photons}} \times 100\% \quad (1)$$

in which $N_{electrons}$, $N_{photons}$, $N_{methanol}$, and $N_{ethanol}$ represent the number of reacted electrons and incident photons, the molecule number of generated methanol and

ethanol, respectively. The number of incident photons was measured by the ferrioxalate actinometer method. In a typical procedure, 6 mL of $Fe_2(SO_4)_3$ solution (0.02 M) were mixed with 6 mL of $Na_2C_2O_4$ solution (0.12 M) and irradiated for 20 s. Afterwards, 1 mL of the resulted solution, 2 mL of 1,10-phenanthrolin solution (0.2 wt %) and 0.5 mL of buffer solution (pH = 4.5, prepared by dissolving 3.36 g of CH_3COONa to 50 mL of H_2SO_4 solution (0.184 M)) were diluted to 100 ml and subsequently kept in the dark under stirring for 30 min. After the reaction, the ferrous ion concentration is subsequently determined via a UV-Vis spectrophotometric determination of its phenanthroline complex at 510 nm. The blank value was measured using the same process without irradiating. The number of incident photons per unit time was calculated as follows,

$$n=\frac{(A_t - A_0)\times V\times N_A}{\varepsilon L \times \phi_{Fe^{2+}} t} \quad (2)$$

in which A and V signify absorbance at 510 nm and corresponding volume of diluted solution (1200 mL), respectively. $N_A=6.02\times10^{23}$, $\varepsilon=1.11\times10^4$ L mol^{-1} cm^{-1}, L=1 cm, φ=1.21, t=20 s. Results show that the number of incident photons (n) was 7.260×10^{16} photons s^{-1}.

II. Supporting Data

A. Characterization of $AgCl_xBr_{1-x}$ NCs

Table S2 Comparison of Cl/Br mole ratios of $AgCl_xBr_{1-x}$ NCs between theoretical values and experimental results.

Samples	AgBr	$AgCl_{0.25}Br_{0.75}$	$AgCl_{0.5}Br_{0.5}$	$AgCl_{0.75}Br_{0.25}$	AgCl
Theoretical value	0:1	1:3	1:1	3:1	1:0
EDX results	0:1	1:2.853	1:1.107	2.714:1	1:0
XPS results	0:1	1:3.179	1:1.142	2.855:1	1:0

Table S3 Crystal structures and photophysical and photocatalytic properties of $AgCl_xBr_{1-x}$ NCs. Lattice constant is obtained based on XRD results. Experimental bandgap values were estimated from UV-Vis DRS results, while the theoretical values are calculated from WIEN2K program (Figure 6 and Figure S8). Photocatalytic performances are evaluated by the MO degradation and CO_2 reduction reaction.

Samples	Lattice constant (Å)	Indirect bandgaps (eV)		Direct bandgaps (eV)		Degradation rate constant (min^{-1})	Apparent quantum efficiency (%)
		exp	cal	exp	cal		
AgBr	5.774	2.48	2.16	3.18	2.86	0.410	2.695
$AgCl_{0.25}Br_{0.7}$	5.746	2.58	2.20	3.25	3.01	0.338	2.101
5							
$AgCl_{0.5}Br_{0.5}$	5.691	2.67	2.22	3.32	3.16	0.487	2.311
$AgCl_{0.75}Br_{0.2}$	5.616	2.89	2.41	3.33	3.39	0.677	3.781

5							
AgCl	5.555	2.99	2.79	3.44	3.59	0.184	1.794

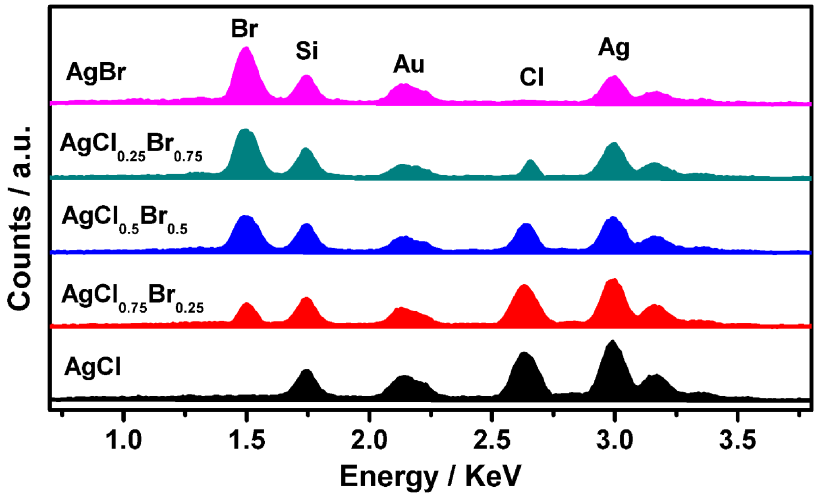

Figure S2 Comparison of the EDAX results of $AgCl_xBr_{1-x}$ samples. The K Peaks at about 11.9 KeV (ascribed to Br) were too weak to differentiate, thus we abandoned it and listed the results at Table S2.

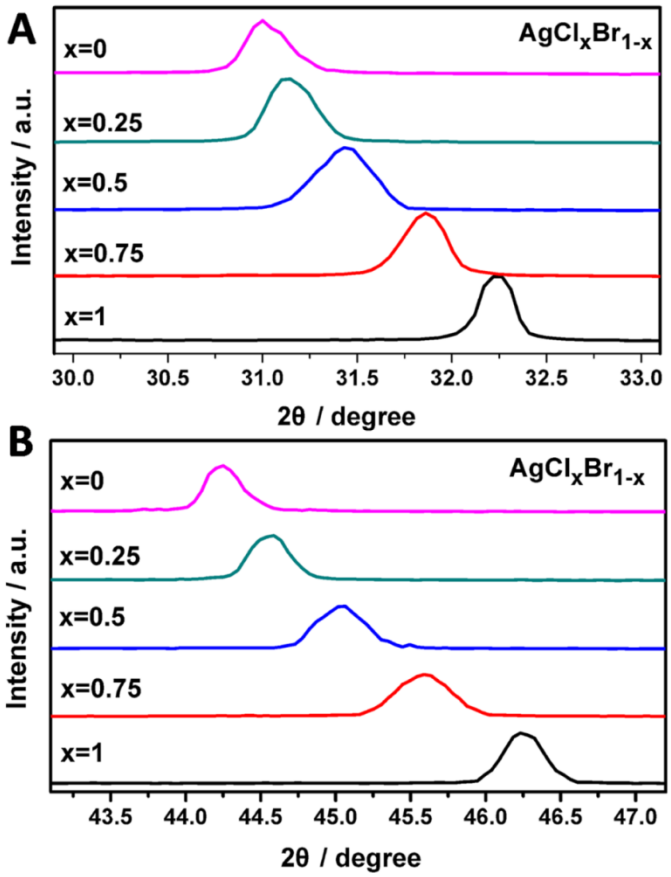

Figure S3 Shifts of A) (200) and B) (220) Bragg's peak for $AgCl_xBr_{1-x}$ NCs with different chemical compositions.

B. Photophysical Properties and Photocatalytic Performance

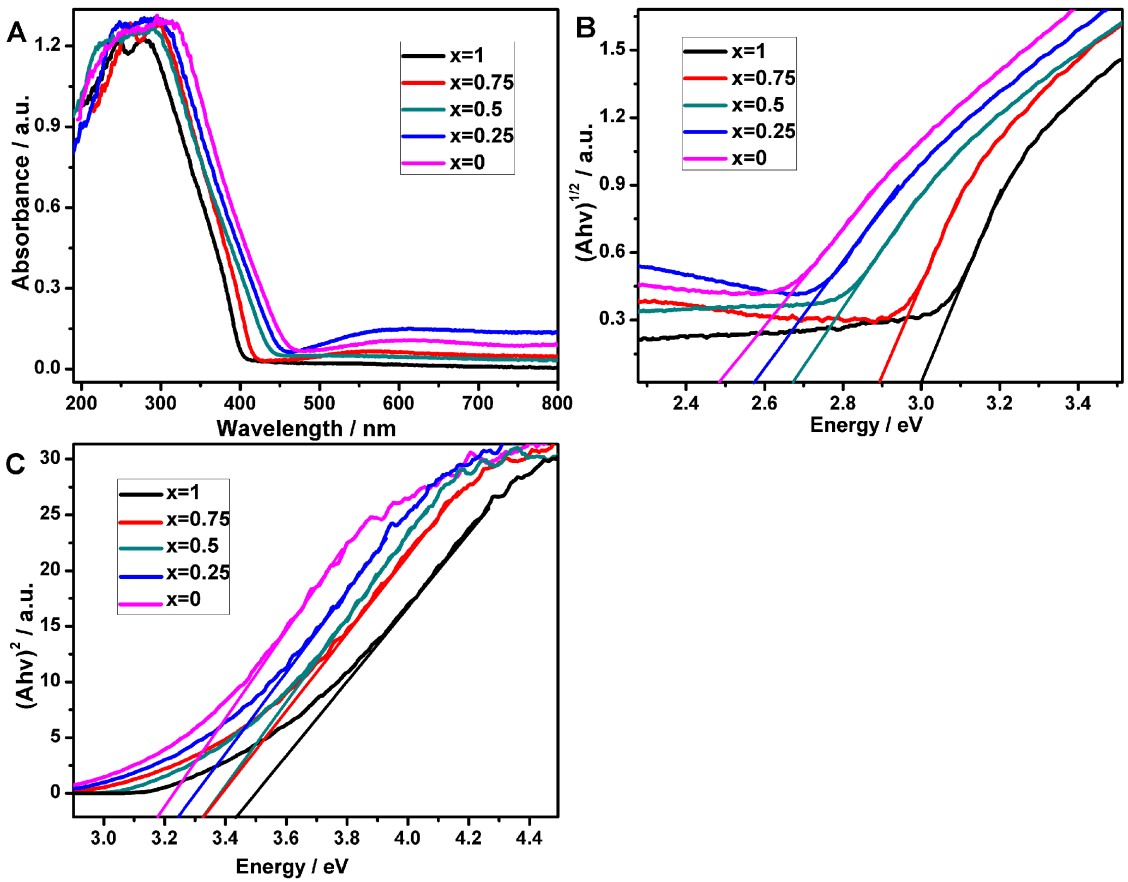

Figure S4 The UV–Vis diffusive reflectance spectra of $AgCl_xBr_{1-x}$ NCs. (A) UV-Vis absorption spectra. (B) Indirect and (C) direct bandgap estimation based on Kubelka-Munk Theory. Since the samples were all synthesized in the dark, the generation of the Ag^0 species could be nearly forbidden. No plasmonic absorption was detected in the UV-Vis absorption spectra (Figure S4 A), which allow the bandgap estimation more accurate. The bandgap values are listed below (Table S3).

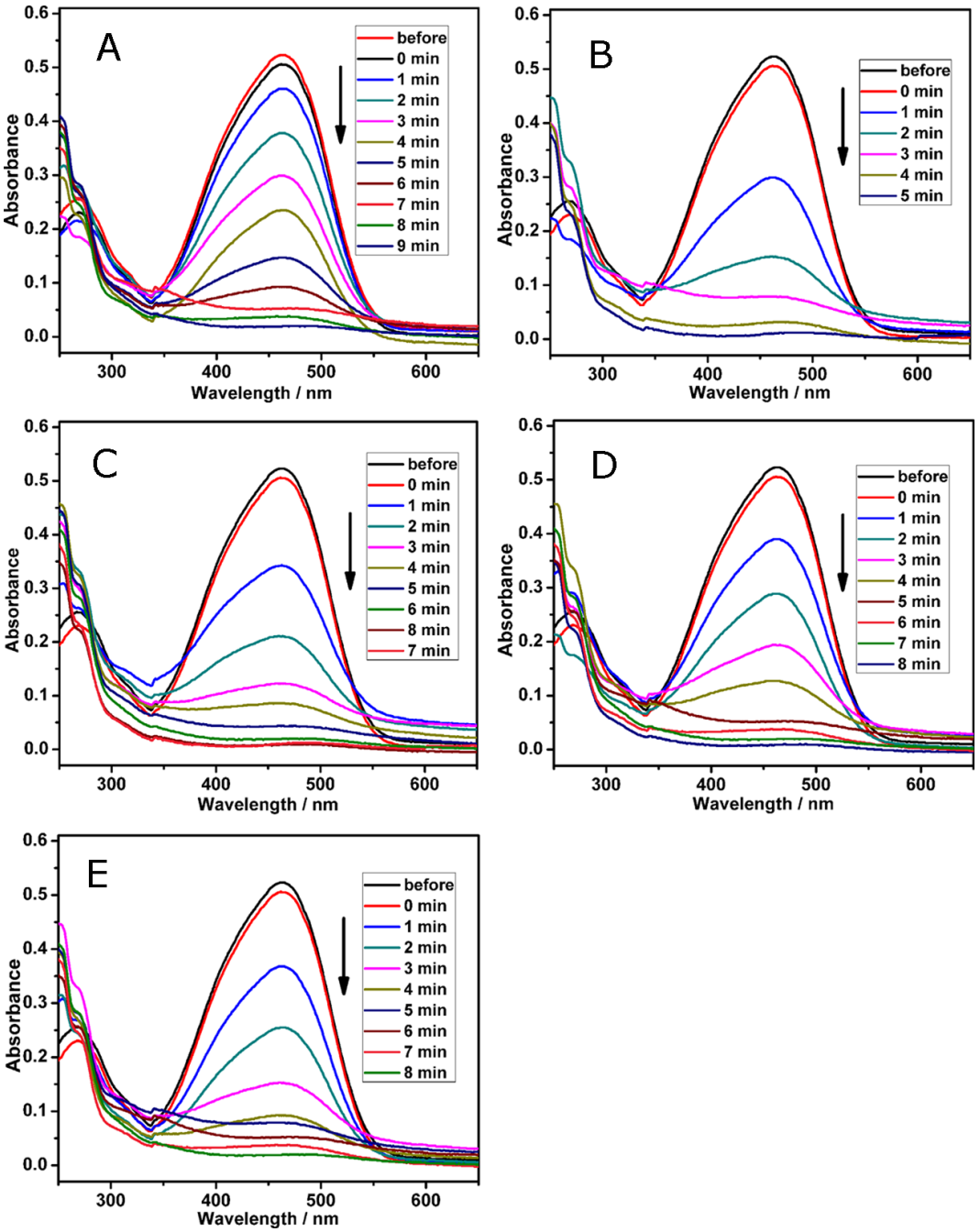

Figure S5. Typical real-time absorption spectra of the MO dye during the photodegradation process over (A) AgCl, (B) $AgCl_{0.75}Br_{0.25}$, (C) $AgCl_{0.5}Br_{0.5}$, (D) $AgCl_{0.25}Br_{0.75}$, (E) AgBr photocatalysts under visible-light irradiation. The black and red curves marked as 'before' and '0 min' in each panel are the absorption spectra detected from the original MO solution before and after the dark adsorption experiment, respectively.

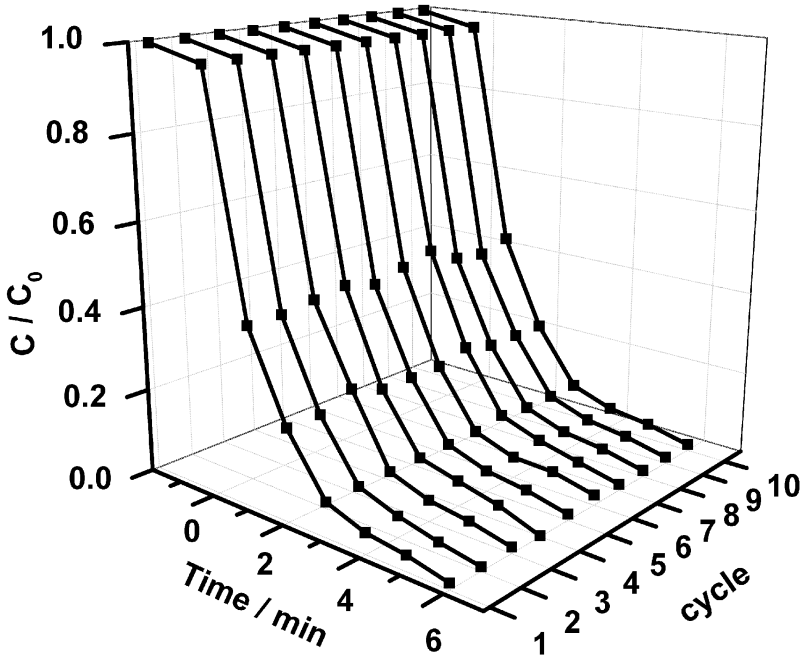

Figure S6 Recycling experiments of $AgCl_{0.75}Br_{0.25}$ samples in the MO degradation reaction.

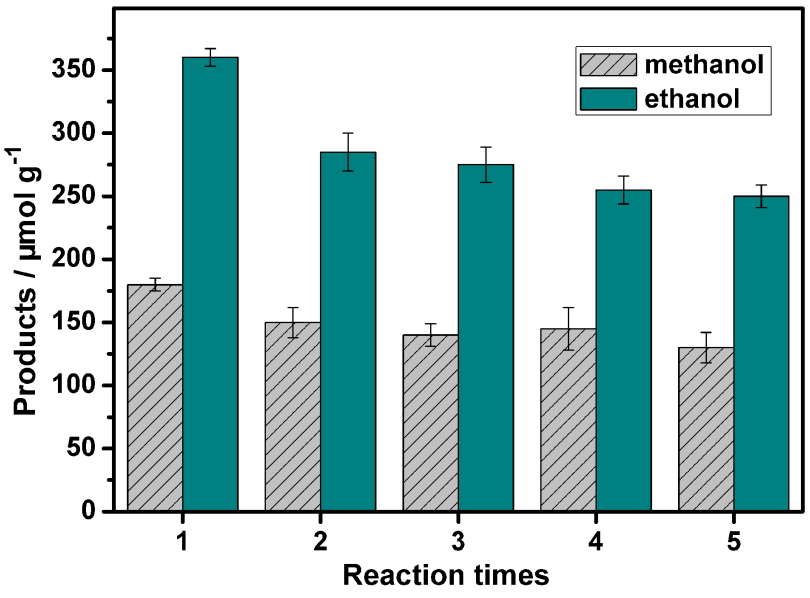

Figure S7 Recycling experiments of $AgCl_{0.75}Br_{0.25}$ samples in the CO_2 reduction reaction.

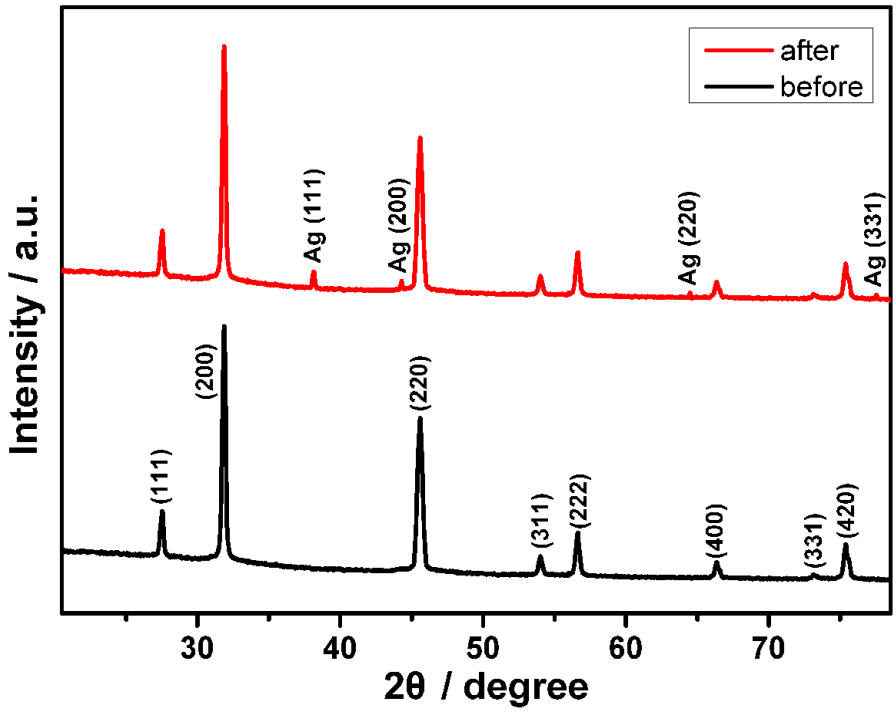

Figure S8 XRD results comparison of the $AgCl_{0.75}Br_{0.25}$ sample before and after the reaction of MO photodegeradation. After the reaction, $AgCl_{0.75}Br_{0.25}$ sample still display similar diffraction peaks (2θ) at 27.5°(111), 31.8°(220), 45.6°(220), 54.0°(311), 56.6°(222), 66.3°(400), 73.2°(331) and 75.4°(420), which illustrates that the crystal structure did not changed significantly. However, the formation of Ag^0 species cannot be avoided because of the LSPR. The diffraction peaks (2θ) at 38.2°(111), 44.3°(200), 38.2°(111), 64.5°(220) and 77.5°(331) are ascribed to the diffractions of the metallic state of Ag (JCPDS file: 65-2871), respectively.

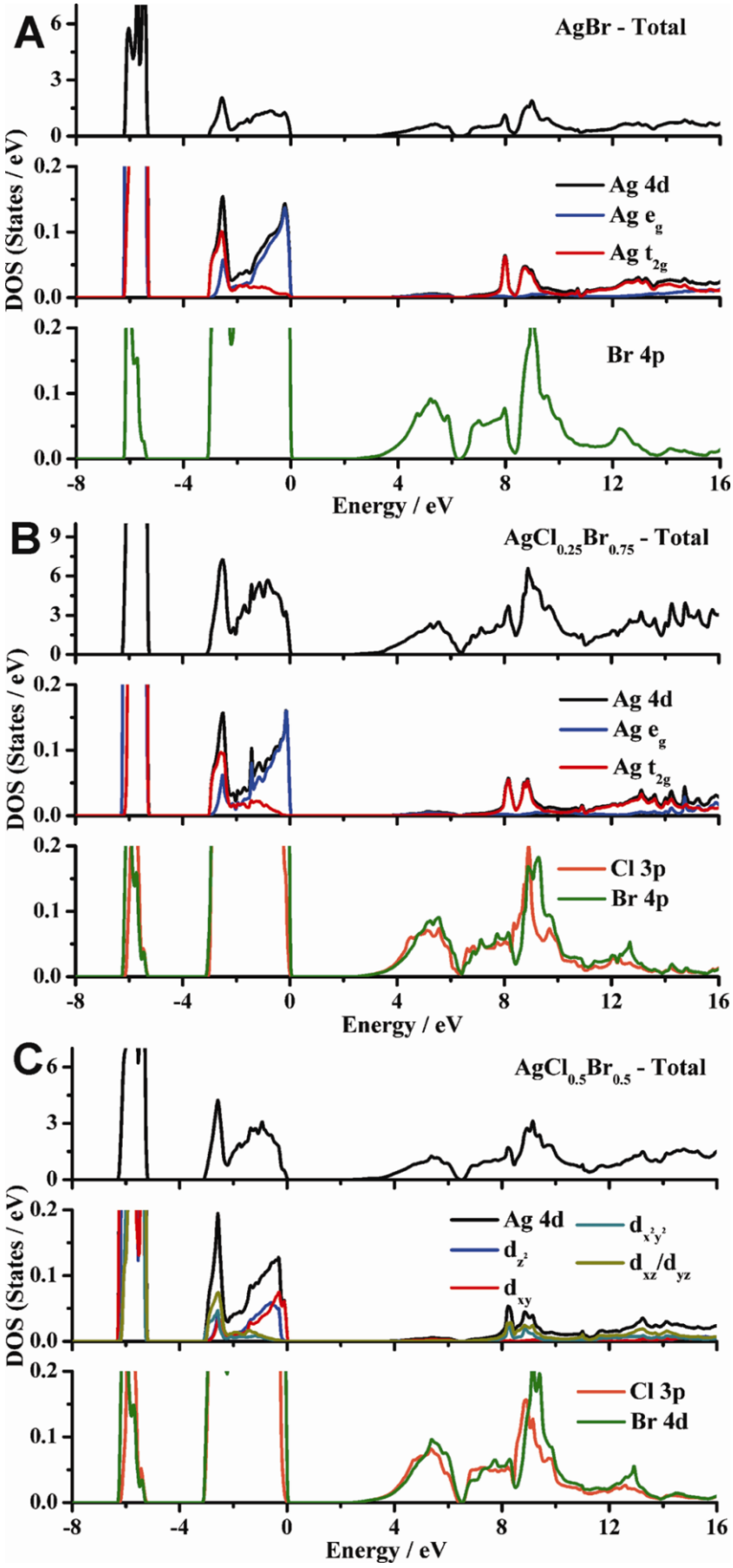

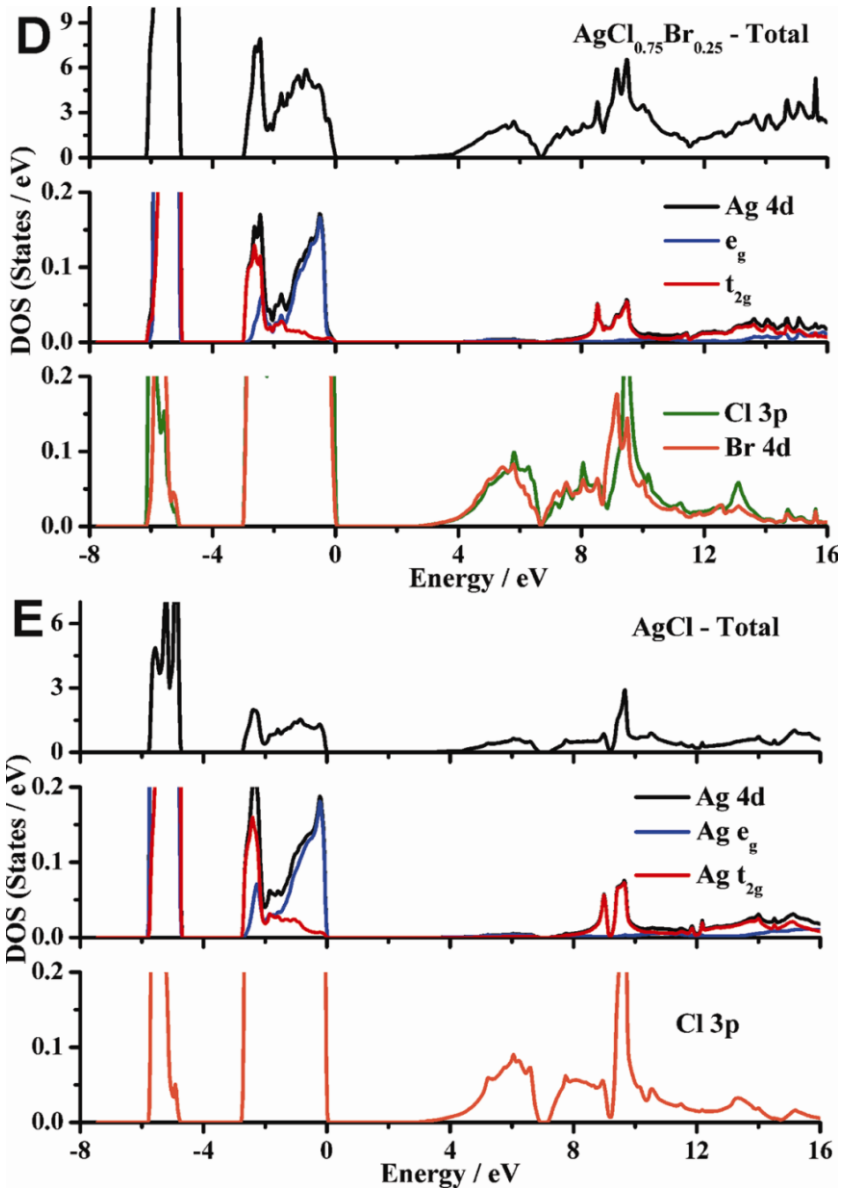

Figure S9 Total and partial density of states for (A) AgBr, (B) $AgCl_{0.25}Br_{0.75}$, (C) $AgCl_{0.5}Br_{0.5}$, (D) $AgCl_{0.75}Br_{0.25}$, (E) AgCl.